A Three-Terminal Approach to Developing Spin-Torque Written Magnetic Random Access Memory Cells

Patrick M. Braganca, Jordan A. Katine, *Senior Member, IEEE*, Nathan C. Emley, Daniele Mauri, Jeffrey R. Childress, *Senior Member, IEEE*, Philip M. Rice, Eugene Delenia, Daniel C. Ralph, and Robert A. Buhrman

***Abstract*—Using a self-aligned fabrication process together with multiple-step aligned electron beam lithography, we have developed a nanopillar structure where a third contact can be made to any point within a thin-film multilayer stack. This substantially enhances the versatility of the device by providing the means to apply independent electrical biases to two separate parts of the structure. Here, we demonstrate a joint magnetic spin-valve (SV)/tunnel junction structure sharing a common free layer nanomagnet contacted by this third electrode. A spatially nonuniform spin-polarized current flowing into the free layer via the low-resistance SV path can reverse the magnetic orientation of the free layer as a consequence of the spin-torque (ST) effect, by nucleating a reversal domain at the spin injection site that propagates across the free layer. The free layer magnetic state can then be read out separately via the higher resistance magnetic tunnel junction (MTJ). This three-terminal structure provides a strategy for developing high-performance ST magnetic random access memory (ST-MRAM) cells, which avoids the need to apply a large voltage across a MTJ during the writing step, thereby enhancing device reliability, while retaining the benefits of a high-impedance MTJ for read-out.**

***Index Terms*—Magnetic memories, magnetic tunnel junctions (MTJs), nanofabrication, spin torque (ST).**

Manuscript received July 24, 2008. First published September 3, 2008; current version published March 6, 2009. This work was supported in part by the Semiconductor Research Corporation (SRC) and in part by the National Science Foundation's Nanoscale Science and Engineering Center (NSF/NSEC) program through the Cornell Center for Nanoscale Systems. The review of this paper was arranged by Associate Editor L. Dong.

P. M. Braganca was with the Department of Applied and Engineering Physics, Cornell University, Ithaca, NY 14853-2501 USA. He is now with the Hitachi Global Storage Technologies, San Jose, CA 95135 USA (e-mail: patrick.braganca@hitachigst.com).

J. A. Katine and J. R. Childress are with the Hitachi Global Storage Technologies, San Jose, CA 95135 USA (e-mail: jordan.katine@hitachigst.com; jeff.childress@hitachigst.com).

N. C. Emley was with the Department of Applied and Engineering Physics, Cornell University, Ithaca, NY 14853 USA. He is now with the Department of Electrical Engineering and Computer Science, University of California Berkeley, Berkeley, CA 94720 USA (e-mail: emley@eecs.berkeley.edu).

D. Mauri was with Hitachi Global Storage Technologies, San Jose, CA 95135 USA. He is now with Western Digital Corporation, Fremont, CA 94539 USA (e-mail: daniele.mauri@gmail.com).

P. M. Rice and E. Delenia are with IBM Almaden Research Center, San Jose, CA 95120 USA (e-mail: pmrice@almaden.ibm.com; edelenia@us.ibm.com).

D. C. Ralph is with the Department of Physics, Cornell University, Ithaca, NY 14853 USA (e-mail: ralph@ccmr.cornell.edu).

R. A. Buhrman is with the Department of Applied and Engineering Physics, Cornell University, Ithaca, NY 14853 USA (e-mail: rab8@cornell.edu).

Color versions of one or more of the figures in this paper are available online at http://ieeexplore.ieee.org.

Digital Object Identifier 10.1109/TNANO.2008.2005187

I. Introduction

RECENT advances in the fabrication of magnetic tunnel junctions (MTJs) with high tunneling magnetoresistance (TMR) have led to the successful development and commercialization of magnetic random access memory [1] (MRAM). This memory technology incorporates fast read/write speeds with low power consumption and nonvolatility, making it suitable for a multitude of applications. Presently, MRAM write schemes involve the use of magnetic fields generated by electric currents to change the free layer magnetic state of MTJs functioning as memory bits. However, this strategy will encounter difficulties with bit selection and power dissipation [2] as the bit size scales to smaller dimensions. An alternative writing scheme [3]–[5] currently being explored involves the use of a spin polarized electrical current to reverse the magnetic bit through an exchange of spin angular momentum, otherwise know as the spin-torque (ST) effect [6]–[9]. In ST devices studied to date, a large voltage must be applied across the MTJ to generate the current densities required for fast ST switching ($\sim 10^6$–10^7 A/cm^2), and this can compromise device reliability due to wear out by dielectric breakdown. Here, we demonstrate a three-terminal device in which a middle electrode can be contacted to a thin magnetic layer that serves simultaneously as a free layer for both an MTJ (on one side of the structure) and an all metallic spin valve (SV) (on the other side). A relatively small voltage applied to the low-resistance SV can drive sufficient current to write the state of the free layer by ST switching, and the free-layer orientation can then be read out separately by the tunnel junction, a strategy that not only eliminates issues arising from MTJ wear out, but also avoids the possibility of inadvertent bit reversal occurring during a read cycle.

II. Device Fabrication

The implementation of our device concept [shown schematically in Fig. 1(a)] involves patterning a nanopillar with exchange-pinned reference layers below (RL1) and above (RL2) a third ferromagnetic free layer (FL) whose magnetic moment is free to rotate and reverse its orientation. We deposited an insulating MgO barrier between RL1 and FL and a Cu spacer layer between FL and RL2, creating a system with an MTJ and an SV sharing a common free layer. Subsequent nanofabrication steps created a middle electrode connected directly to the free layer, so that simultaneous, independent measurements could be made of the MTJ and SV. ST effects occur by flowing current

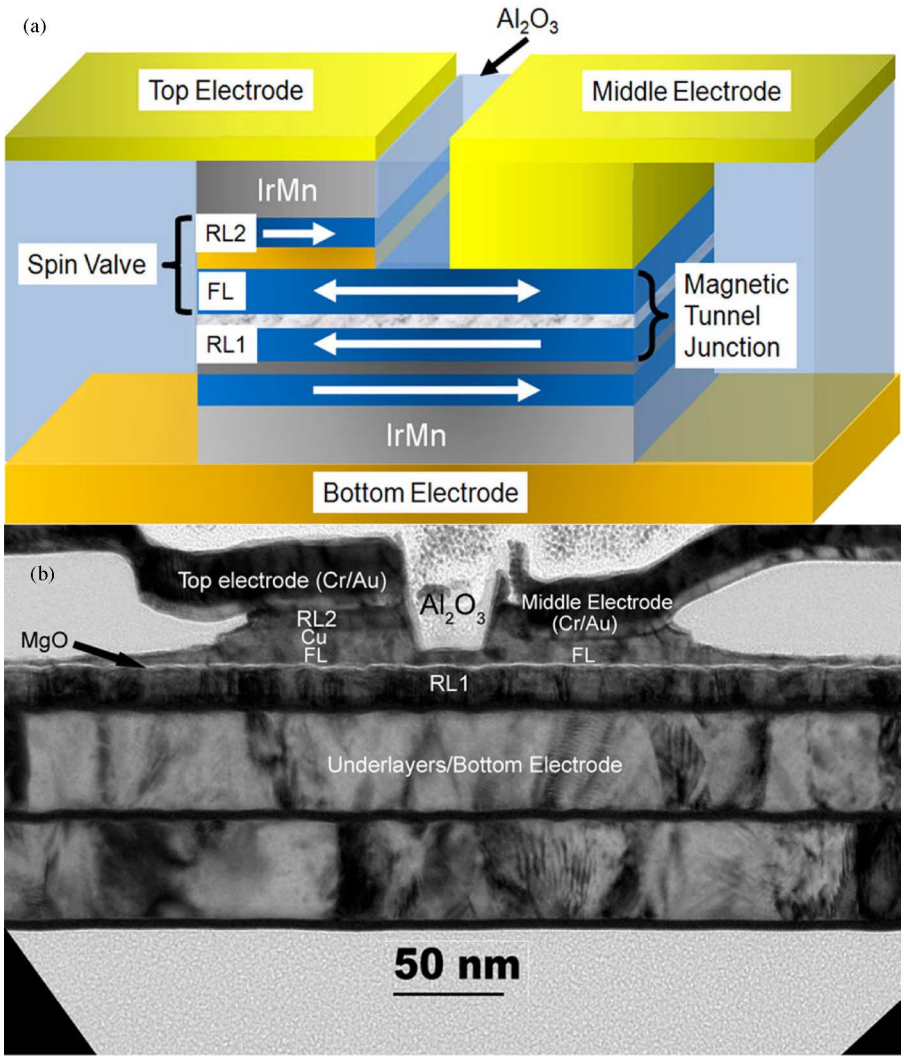

Fig. 1. (color online) (a) Concept for a three-terminal nanopillar structure—a combination SV/MTJ device sharing a common magnetic free layer (FL). Current passed between the top and middle electrode can reverse the magnetization of this common layer through ST, while detection of a reversal is achieved by measuring the resistance of the MTJ between the middle and bottom electrodes. This read/write strategy eliminates barrier breakdown issues with the MTJ. The magnetizations of the SV and MTJ reference layers are pinned AP with respect to one another. (b) TEM cross section of an EBL-defined test structure patterned simultaneously with the elliptical devices.

between the top and middle electrodes, such that electrons flow through RL2 and laterally across the free layer in order to reach the middle electrode.

We began the fabrication process by sputter depositing a multilayer stack of a thick bottom electrode (Ta/Cu/Ta/Cu/Ta/Ru)/60 IrMn/18 CoFe/4 Ru/20 CoFeB/MgO/5 CoFe/60 NiFe/10 CoFe/32 Cu/25 CoFe/60 IrMn/60 Ru where all thicknesses are in angstrom. The bottom IrMn/CoFe/Ru/CoFeB layers form a synthetic antiferromagnet (SAF) that acts to provide both strong pinning for the bottom reference layer (RL1) and to promote the growth of the ultrathin MgO barrier, resulting in a barrier resistance-area (RA) product of $\sim 3\ \Omega \cdot \mu m^2$. A CoFe/NiFe bilayer was chosen for the free layer material because previous studies [10], [11] on ferromagnets with low saturation magnetization M_s have shown substantial reductions in the current required for ST reversal, although we have found that this choice, coupled with the low RA barrier, resulted in a device with relatively low TMR ($\sim$6%). The top CoFe reference layer (RL2) was stabilized by exchange bias with the top IrMn layer; because RL1 is antiparallel (AP) pinned and RL2 is simple pinned, the magnetization of RL2 is AP to RL1. Electron beam lithography (EBL) and Ar^+ ion milling were then used to pattern elliptical nanopillars similar to those shown in Fig. 2(a), and standard photolithography was used to pattern the bottom electrode. A self-aligned process [12] insulated the nanopillar sidewalls with Al_2O_3 while still allowing for contacts to be made to the top of the device.

To pattern the top and middle electrodes, aligned EBL was used to define a 40-nm-wide trench separating the right and left sides of the ellipse, as shown in Fig. 2(b). The e-beam resist [polymethyl-methacrylate (PMMA)] served as both a milling mask and as a lift-off mask for the subsequent alumina deposition. Ion milling was terminated when the free layer was reached, and the resulting trench was refilled with alumina without

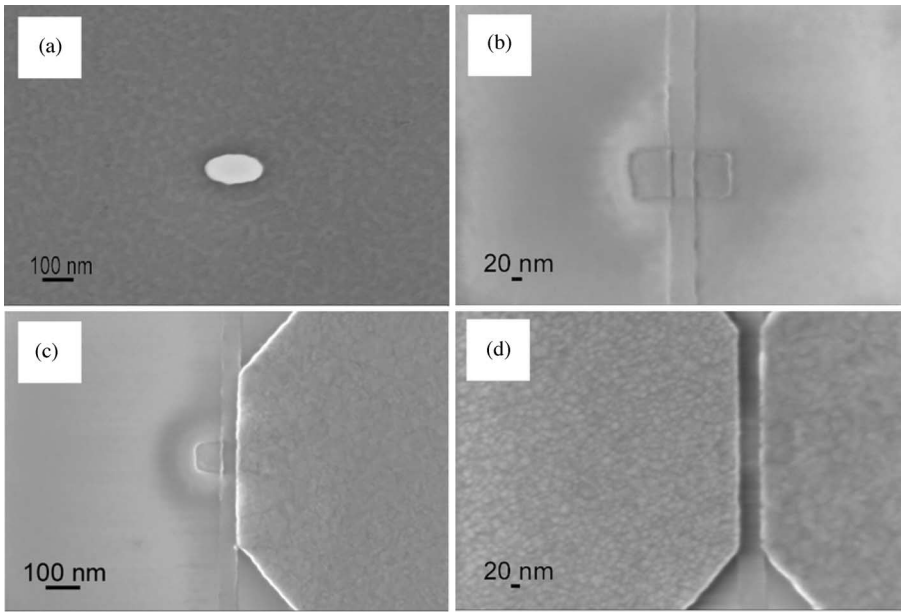

Fig. 2. Scanning electron micrographs at different stages of three-terminal processing. (a) Nanopillar has been defined with an elliptical shape using EBL and ion milling. (b) Using aligned EBL, a ~40 nm trench has been milled out of the center of the ellipse, down to the free layer of the device. This trench is then refilled with alumina to isolate the left edge of the ellipse from the right. (c) Aligned EBL defines the right contact, which was milled to the free layer before depositing the Cr/Au contact. (d) One final aligned EBL allows for deposition of the left Cr/Au contact.

breaking vacuum. Low voltage (175 V) Ar^+ ion milling insured that the free layer would be undamaged by our processing and provided the slow etch rate required to control the milling depth. Because they were milled to different depths in order to contact the middle and top electrodes, separate aligned EBL steps defined the right [see Fig. 2(c)] and left contacts [see Fig. 2(d)]. For both sides, the ion mills were followed by *in situ* 50 Cr/200 Au depositions to insure good electrical contact. Fig. 1(b) shows a cross-sectional transmission electron microscopy (TEM) image taken from the center of a 4-μm-long, 200-nm-wide test device processed in the same manner as the elliptical devices. These long devices make TEM sample preparation far easier than it is for the actual ellipses. Here, we note that both the insulating trench and the right contact have been milled to the top of the NiFe layer directly above the MgO barrier (which appears as a thin white line), demonstrating that the electrodes can be controllably placed anywhere within the multilayer stack. The tapered sidewalls of the layers above the MgO barrier seen in Fig. 1(b) result from shadowing effects during ion milling that are accentuated by the length of the 4-μm-long test line. There is significantly less shadowing in the case of the small elliptical patterns; so, we are confident that the actual devices have been cleanly milled down past the MgO layer.

III. Micromagnetic Simulations

To develop an understanding of the ST-driven reversal process in this novel nanopillar system, we used a three-dimensional (3-D) zero temperature micromagnetic simulation package [7], [11], [13] that includes the Slonczewski ST term. Fig. 3(a) shows the initial state of the free layer, where to simplify our calculations, the magnet has been assumed to be a 40×142.5 nm^2 rectangle and the Oersted field generated by the applied current has not been considered. For simplicity, we also considered only the ST transmitted by the current flowing perpendicular to the films, so that ST is locally exerted at the interface of the free layer directly below RL2, as noted by the outlined region in Fig. 3(a). In principle, one should also take into account additional ST interactions between the current flowing laterally across the free layer and any domain walls formed in that layer (the domain-wall drag effect) [14]–[19]. However, we will argue later that this effect is negligible in our devices. Fig. 3(b)–(e) demonstrates the evolution of the reversal process for a -3 mA current spin-polarized AP to the initial magnetization of the free layer. Switching is initiated by the formation of a reversal domain beneath RL2, creating a head-to-head 180° domain wall within the free layer. This domain wall then propagates toward the right end of the free layer driven by exchange force, reflects off the right edge of the magnet, and decays rapidly away as it travels back toward the left edge, where the magnetization is stabilized by the ST exerted on that region. Similar simulation results are obtained for the switching of the free layer magnetization from an orientation parallel to RL2 to one AP by the ST exerted by electrons flowing from the free layer to RL2. By comparing these results to simulations with the ST exerted on the entire free layer (i.e., as in uniform current injection into a simple SV structure), we find that the current amplitudes required for magnetization reversal are essentially the same, indicating that there should be no loss of ST efficiency from the nonuniform localized current injection in this three-terminal device geometry.

IV. Results and Discussion

Before fabricating and testing a complete three-terminal ST device structure, we used a simplified multilayer stack of

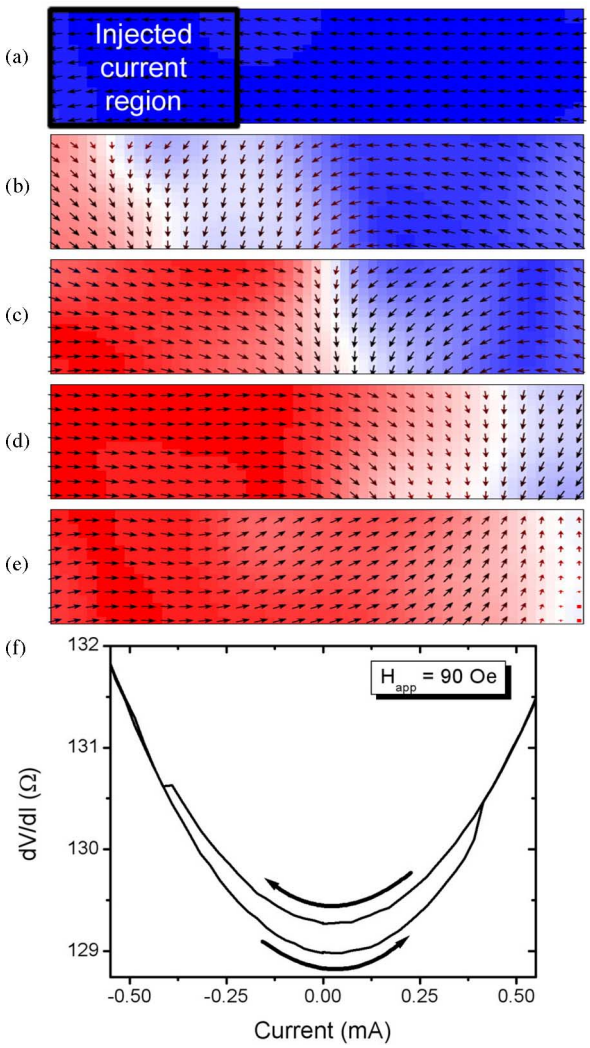

Fig. 3. (color online) (a)–(e) Zero temperature 3-D micromagnetic simulations of the SV component of the structure. The initial micromagnetic state of a 40×142.5 nm^2 rectangular nanomagnet is shown in (a) with the region where current is injected perpendicular to the film plane indicated, simulating the reference layer in the left contact shown in Fig. 1(a). For a -3 mA current spin-polarized AP to the initial magnetization, a reversal domain forms underneath the reference layer (b), and sweeps across the free layer (c)–(e). (f) Resistance versus current for a 70×200 nm^2 elliptical SV patterned with top and middle electrodes shown in Fig. 1(a). Here, we see that, in fact, the mechanism shown in (a)–(e) is successful in yielding ST reversal. The parabolic background is due to heating.

30 Ta/60 NiFe/10 CoFe/30 Cu/25 CoFe/60 IrMn/60 Ru. These devices do not have a bottom tunnel junction, but were otherwise identical in design to the three-terminal devices, allowing us to use the middle and top electrodes to verify the ST effects in the SV component of the structure. Fig. 3(f) shows a typical resistance versus dc current scan measured at room temperature using standard ac lock-in techniques for a 70×200 nm^2 elliptical nanopillar processed as described before. During the scan, we apply a constant magnetic field to cancel the small dipole field exerted by the reference layer upon the free layer. Due to the narrow channel in the NiFe layer beneath the isolation trench, the resistance of the SV is significantly larger than is typically observed for current perpendicular to the plane SVs. We have verified that the current switches the full area of the free layer (and not just the part under RL2) by using an applied magnetic field to set the initial state of the free layer to both the parallel and antiparallel states; the critical currents shown in Fig. 3(f) are the same in both cases. Assuming that the left contact area has an area half that of the ellipse minus half the area of the isolating trench ($\sim 4.1 \times 10^{-11}$ cm^2), the switching currents shown in Fig. 3(f) correspond to $J_{c,\mathrm{SV}} \approx 1.2 \times 10^7$ A/cm^2, in reasonable agreement with previous ST results in simple SV structures. This is somewhat surprising in that it suggests that the exchange coupling of the rest of the free layer to the area under the SV contact does not substantially impede the reversal process. We will return to this point in the discussion later.

We note in Fig. 3(f) that the critical current amplitude for the AP to parallel (P) transition (high to low resistance) is very similar to that for the P-to-AP transition. Since any domain drag effect from current flowing laterally within the free layer would decrease the critical current for the AP-to-P transition and increase it for the P-to-AP case, our results indicate that ST effects on the domain wall propagation are not significant in this device configuration. We conclude that in this device, the ST due to current flow across a nonferromagnet–ferromagnet interface is much more efficient than that due to current flow through a domain wall.

Fig. 4 shows experimental results for a complete SV/MTJ coupled structure patterned into a 70×200 nm^2 ellipse and processed as described earlier. Measurement of the SV resistance was accomplished using standard ac lock-in techniques, while the dc resistance of the MTJ was measured simultaneously with a multimeter. By varying the applied magnetic field [see Fig. 4(a)], we observe steps in resistance in both the SV and MTJ, corresponding to magnetization reversal of the free layer. Due to the AP alignment of RL1 and RL2 with respect to one another, a switch to the high-resistance state of the SV corresponds to a switch to the low-resistance state of the MTJ.

In Fig. 4(b), we show the results of applying dc current through the SV while reading the resistance of the MTJ. ST reversal occurs from the high- to low-resistance state with respect to the SV, and is simultaneously detected by the MTJ. The resistance change of the MTJ initiated by the ST effect is equal to the magnetoresistance change observed by sweeping the field, which confirms that the ST effect reverses the entire free layer, as predicted by the micromagnetic simulation, and does not result in the formation of a stable domain wall in the free layer, which would result in an intermediate resistance level in the MTJ. We were not able to reverse the SV device configuration from the P-to-AP state by flowing current in the positive direction (electrons from free layer to RL2) due to the fact that before the critical current was reached, the circumferential Oersted field acting on RL2 due to the applied current became strong enough to overcome the exchange pinning field from the top IrMn layer and drive the magnetization of the approximately square RL2 into a vortex state. The spin-polarized current generated from such a reference layer configuration is insufficient for reversing the free layer, since STs exerted in different spatial regions tend to cancel each other out. The formation of the vortex state occurs because the reversal currents required in the full three-terminal

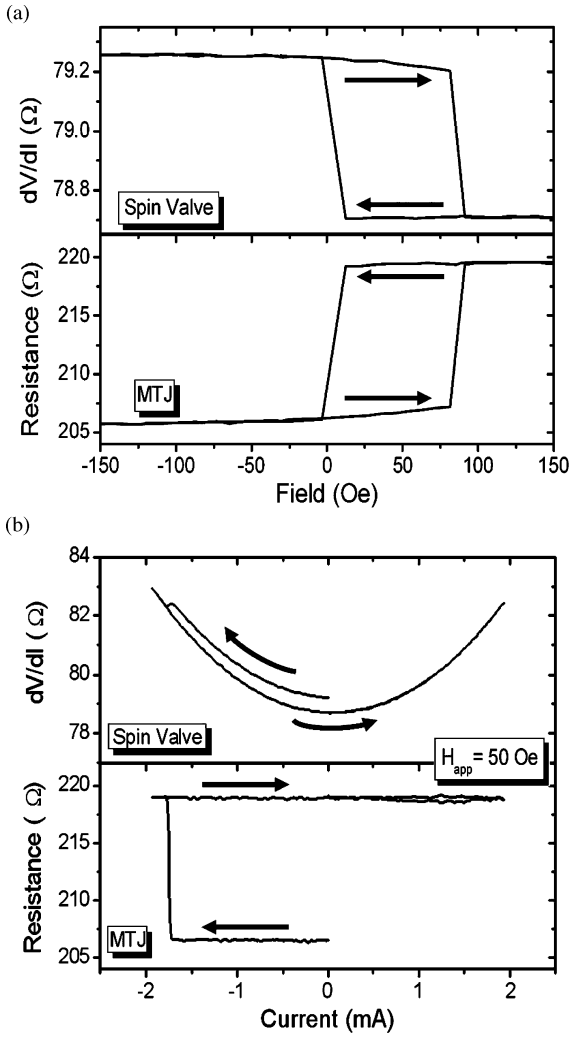

Fig. 4. (a) Resistance versus magnetic field measured simultaneously for both the SV and MTJ in a completed device. The steps in resistance correspond to reversal of the free layer detected using the giant magnetoresistance (in the SV) and TMR effects. Since RL1 and RL2 are pinned AP with respect to each other, the high-resistance state of the SV is the low-resistance state of the MTJ. (b) Resistance versus current measured simultaneously for the full three-terminal SV/MTJ. ST in this device can drive the AP-to-P transition within the SV, but not the P-to-AP transition, because a vortex forms in RL2 prior to free layer reversal for P-to-AP, due to the large currents required for reversal in this structure.

structures are considerably larger than observed in the isolated SV structure measured in Fig. 3(f). We attribute this difference to an over milling of the isolation trench in the isolated SV structure, resulting in a thinner NiFe channel connecting the left and right ends of the free layer than in the full three-terminal device. As a result, the resistance of the isolated SV structure is found to be ∼40% larger than the SV component of the full three-terminal device, as seen in comparing Fig. 3(f) to Fig. 4. We expect thermal effects to play a more significant role in reducing switching currents for the isolated SV structures due to the higher device resistance and lack of a bottom electrode to conduct away heat. This partially etched trench also weakens the net exchange coupling between free layer material under the SV contact and the rest of the free layer, which, as indicated by our micromagnetic modeling, can substantially reduce the switching current required to nucleate and propagate the domain wall in the isolated SV.

V. Conclusion

In conclusion, we have demonstrated a fabrication concept for inserting a third electrode into a nanopillar device, so that contact can be made to any layer within the pillar. Fabrication of these devices has allowed us to study ST-driven switching by nonuniform current injection into one side of a magnetic free layer. Based on micromagnetic modeling, we argue that this switching occurs by the nucleation of a reversed domain under the contact region, and then, propagation of a domain wall through the rest of the layer driven by the pressure of the exchange field. ST from the spin current traveling laterally through the free layer appears to have minimal effect on the reversal process. Free layer reversal initiated by injecting current through the SV can be detected by the resultant resistance change in the MTJ, allowing for an ST writing scheme without tunnel barrier wear out issues while retaining the benefits for read-out of the large TMR signals from MTJs. Further optimization of this system requires improving the resistance of the top reference layer RL2 to vortex-state formation by enhancing its exchange bias pinning and/or its geometry, fabricating the MTJ with a much better TMR and a higher, more appropriate resistance ($\geq$3000 Ω) for impedance matching to a CMOS sense transistor, and choosing the free layer material, thickness, and trench etch depth, so as to minimize the SV reversal currents while maintaining good thermal stability. This three-terminal structure offers exiting new opportunities for examining physical effects in magnetic systems, while also providing a possible architecture for future high-performance, high-speed ST-MRAM applications.

References

[1] M. Durlam, D. Addie, J. Akerman, B. Butcher, P. Brown, J. Chan, M. DeHerrera, B. N. Engel, B. Feil, G. Grynkewich, J. Janesky, M. Johnson, K. Kyler, J. Molla, J. Martin, K. Nagel, J. Ren, N. D. Rizzo, T. Rodriguez, L. Savtchenko, J. Salter, J. M. Slaughter, K. Smith, J. J. Sun, M. Lien, K. Papworth, P. Shah, W. Qin, R. Williams, L. Wise, and S. Tehrani, "A 0.18 μm 4 Mb toggling MRAM," *IEEE IEDM*, pp. 995–997, Dec. 2003.

[2] J. A. Katine and E. E. Fullerton, "Device implications of spin-transfer torques," *J. Magn. Magn. Mater.*, vol. 320, pp. 1217–1226, Apr. 2008.

[3] F. J. Albert, J. A. Katine, R. A. Buhrman, and D. C. Ralph, "Spin-polarized current switching of a Co thin film nanomagnet," *Appl. Phys. Lett.*, vol. 77, pp. 3809–3811, Dec. 2000.

[4] M. Hosomi, H. Yamagishi, T. Yamamoto, K. Bessho, Y. Higo, K. Yamane, H. Yamada, M. Shoji, H. Hachino, C. Fukumoto, H. Nagao, and H. Kano, "A novel nonvolatile memory with spin torque transfer magnetization switching: Spin-ram," *IEDM Techn. Dig.*, pp. 459–462, Dec. 2005.

[5] T. Kawahara, R. Takemura, K. Miura, J. Hayakawa, S. Ikeda, Y. Lee, R. Sasaki, Y. Goto, K. Ito, I. Meguro, F. Matsukura, H. Takahashi, H. Matsuoka, and H. Ohno, "2 Mb spin-transfer torque RAM (SPRAM) with bit-by-bit bidirectional current write and parallelizing-direction current read," *ISSCC Dig.*, pp. 480–481, 2007.

[6] L. Berger, "Emission of spin waves by a magnetic multilayer traversed by a current," *Phys. Rev. B*, vol. 54, pp. 9353–9358, Oct. 1996.

[7] J. C. Slonczewski, "Current-driven excitation of magnetic multilayers," *J. Magn. Magn. Mater.*, vol. 159, pp. L1–L7, Jun. 1996.

[8] M. Tsoi, A. G. Jansen, J. Bass, W.-C. Chiang, M. Seck, V. Tsoi, and P. Wyder, "Excitation of a magnetic multilayer by an electric current," *Phys. Rev. Lett.*, vol. 80, pp. 4281–4284, May 1998.

[9] J. A. Katine, F. J. Albert, R. A. Buhrman, E. B. Myers, and D. C. Ralph, "Current-driven magnetization reversal and spin-wave excitations in Co/Cu/Co pillars," *Phys. Rev. Lett.*, vol. 84, pp. 3149–3152, Apr. 2000.

[10] P. M. Braganca, I. N. Krivorotov, O. Ozatay, A. G. F. Garcia, N. C. Emley, J. C. Sankey, D. C. Ralph, and R. A. Buhrman, "Reducing the critical current for short-pulse spin-transfer switching of nanomagnets," *Appl. Phys. Lett.*, vol. 87, pp. 112507–112509, Sep. 2005.

[11] P. M. Braganca, O. Ozatay, A. G. F. Garcia, O. J. Lee, D. C. Ralph, and R. A. Buhrman, "Enhancement in spin-torque efficiency by nonuniform spin current generated within a tapered nanopillar spin valve," *Phys. Rev. B*, vol. 77, pp. 144423-1–144423-6, Apr. 2008.

[12] J. R. Childress, M. J. Carey, M.-C. Cyrille, K. Carey, N. Smith, J. A. Katine, T. D. Boone, A. A. G. Driskill-Smith, S. Maat, K. Mackay, and C. H. Tsang, "Fabrication and recording study of all-metal dual-spin-valve CPP read heads," *IEEE Trans. Magn.*, vol. 42, no. 10, pp. 2444–2446, Oct. 2006.

[13] M. J. Donohue and D. G. Porter, *OOMMF Users Guide, Version 1.0, Technical Report No. NISTIR 6376,* National Institute of Standards and Technology, Gaithersburg, MD, 1999.

[14] L. Berger, "Exchange interaction between ferromagnetic domain-wall and electric-current in very thin metallic-films," *J. Appl. Phys.*, vol. 55, pp. 1954–1956, Mar. 1984.

[15] P. P. Freitas and L. Berger, "Observation of s–d exchange force between domain-walls and electric-current in very thin permalloy-films," *J. Appl. Phys.*, vol. 57, pp. 1266–1269, Feb. 1985.

[16] C. Y. Hung and L. Berger, "Exchange forces between domain-wall and electric-current in permalloy-films of variable thickness," *J. Appl. Phys.*, vol. 63, pp. 4276–4278, Apr. 1988.

[17] M. Hayashi, L. Thomas, Y. B. Bazaliy, C. Rettner, R. Moriya, X. Jiang, and S. S. P. Parkin, "Influence of current on field-driven domain wall motion in permalloy nanowires from time resolved measurements of anisotropic magnetoresistance," *Phys. Rev. Lett.*, vol. 96, pp. 197207-1–197207-4, May 2006.

[18] Z. Li and S. Zhang, "Domain-wall dynamics and spin-wave excitations with spin-transfer torques," *Phys. Rev. Lett.*, vol. 92, pp. 207203-1–207203-4, May 2004.

[19] Z. Li and S. Zhang, "Domain-wall dynamics driven by adiabatic spin-transfer torques," *Phys. Rev. B*, vol. 70, pp. 024417-1–024417-10, Jul. 2004.

Authors' photographs and biographies not available at the time of publication.